Aluminum based structures for manipulating short visible wavelength in-plane surface plasmon polariton propagation

Zhengji Xu,[1] Landobasa Y. M. Tobing,[1] Yiyang Xie,[1] Jinchao Tong,[1] Peinan Ni,[1] Shupeng Qiu,[1] Ting Yu[2] and Dao Hua Zhang,[1,*]

[1] OPTIMUS, School of Electrical & Electronic Engineering, Nanyang Technological University, 50 Nanyang Avenue, 639798, Singapore

[2]School of Physical and Mathematical Sciences, Nanyang Technological University, 21 Nanyang Link, 637371, Singapore

**edhzhang@ntu.edu.sg*

Abstract: We report aluminum based structures for manipulation of surface plasmon polariton (SPP) propagation at short wavelength range. Our simulation shows that aluminum is a good metal to excite and propagate SPPs with blue light and that the SPP wavelength can be reduced from about 465 nm to about 265 nm by monitoring the thickness of a coated Si_3N_4 layer above the aluminum film. It is also shown that the damping becomes more significant with the increase of the thickness of the Si_3N_4 layer. We also experimentally demonstrated the SPP wavelength tuning effect for 20nm Si_3N_4 layer covered Al, which can be explained by the variation of effective permittivity. The proposed Metal-Insulator-Air (MIA) structures with SPP wavelength tuning ability have potential applications in 2D optics.

OCIS codes: (240.6680) Surface plasmons; (310.1860) Deposition and fabrication; (260.2065) Effective medium theory; (180.4243) Near-field microscopy.

References and links

1. N. Yu, P. Genevet, M. A. Kats, F. Aieta, J.-P. Tetienne, F. Capasso, and Z. Gaburro, "Light propagation with phase discontinuities: generalized laws of reflection and refraction," Science **334**(6054), 333–337 (2011).
2. Y. Liu and X. Zhang, "Metasurfaces for manipulating surface plasmons," Appl. Phys. Lett. **103**(14), 141101 (2013).
3. L. Y. M. Tobing, L. Tjahjana, D. H. Zhang, Q. Zhang, and Q. Xiong, "Deep subwavelength fourfold rotationally symmetric split-ring-resonator metamaterials for highly sensitive and robust biosensing platform," Sci. Rep. **3**, 2437 (2013).
4. Z. Xu, T. Li, D.-H. Zhang, C. Yan, D. Li, L. Y. M. Tobing, F. Qin, Y. Wang, X. Shen, and T. Yu, "Groove-structured metasurfaces for modulation of surface plasmon propagation," Appl. Phys. Express **7**(5), 052001 (2014).
5. L. Y. M. Tobing, L. Tjahjana, D. H. Zhang, Q. Zhang, and Q. Xiong, "Sub-100-nm sized silver split ring resonator metamaterials with fundamental magnetic resonance in the middle visible spectrum," Adv. Opt. Mater. **2**(3), 280–285 (2014).
6. X. Zhang and Z. Liu, "Superlenses to overcome the diffraction limit," Nat. Mater. **7**(6), 435–441 (2008).
7. X. Yang, D. H. Zhang, Z. Xu, Y. Wang, and J. Wang, "Designing arbitrary nanoscale patterns by a nanocavity waveguide with omnidirectional illumination," Appl. Phys. B **109**(2), 215–219 (2012).
8. J. Wang, F. Qin, D. Hua Zhang, D. Li, Y. Wang, X. Shen, T. Yu, and J. Teng, "Subwavelength superfocusing with a dipole-wave-reciprocal binary zone plate," Appl. Phys. Lett. **102**(6), 061103 (2013).
9. C. Min, Z. Shen, J. Shen, Y. Zhang, H. Fang, G. Yuan, L. Du, S. Zhu, T. Lei, and X. Yuan, "Focused plasmonic trapping of metallic particles," Nat. Commun. **4**, 2891 (2013).
10. C. Yan, D. H. Zhang, D. Li, H. Bian, Z. Xu, and Y. Wang, "Metal nanorod-based metamaterials for beam splitting and a subdiffraction-limited dark hollow light cone," J. Opt. **13**(8), 085102 (2011).
11. Y. Wang, D. H. Zhang, J. Wang, X. Yang, D. Li, and Z. Xu, "Waveguide devices with homogeneous complementary media," Opt. Lett. **36**(19), 3855–3857 (2011).
12. Y. Luo, D. Y. Lei, S. A. Maier, and J. B. Pendry, "Transformation-Optics Description of Plasmonic nanostructures containing blunt edges/corners: from symmetric to asymmetric edge rounding," ACS Nano **6**(7), 6492–6506 (2012).

#243719 Received 30 Jun 2015; revised 2 Aug 2015; accepted 14 Aug 2015; published 21 Aug 2015

13. L. Huang, X. Chen, B. Bai, Q. Tan, G. Jin, T. Zentgraf, and S. Zhang, "Helicity dependent directional surface plasmon polariton excitation using a metasurface with interfacial phase discontinuity," Light Sci. Appl. **2**(3), e70 (2013).
14. J. Lin, J. P. Mueller, Q. Wang, G. Yuan, N. Antoniou, X.-C. Yuan, and F. Capasso, "Polarization-controlled tunable directional coupling of surface plasmon polaritons," Science **340**(6130), 331–334 (2013).
15. Q. Wang, J. Bu, and X. C. Yuan, "High-resolution 2D plasmonic fan-out realized by subwavelength slit arrays," Opt. Express **18**(3), 2662–2667 (2010).
16. B. Gjonaj, A. David, Y. Blau, G. Spektor, M. Orenstein, S. Dolev, and G. Bartal, "Sub-100 nm focusing of short wavelength plasmons in homogeneous 2D space," Nano Lett. **14**(10), 5598–5602 (2014).
17. L. Li, T. Li, S. M. Wang, C. Zhang, and S. N. Zhu, "Plasmonic Airy beam generated by in-plane diffraction," Phys. Rev. Lett. **107**(12), 126804 (2011).
18. G. Maidecchi, G. Gonella, R. Proietti Zaccaria, R. Moroni, L. Anghinolfi, A. Giglia, S. Nannarone, L. Mattera, H.-L. Dai, M. Canepa, and F. Bisio, "Deep ultraviolet plasmon resonance in aluminum nanoparticle arrays," ACS Nano **7**(7), 5834–5841 (2013).
19. W. Su, G. Zheng, and X. Li, "Design of a highly sensitive surface plasmon resonance sensor using aluminum-based diffraction grating," Opt. Commun. **285**(21-22), 4603–4607 (2012).
20. K.-H. Lee and K. J. Chang, "First-principles study of the optical properties and the dielectric response of Al," Phys. Rev. B Condens. Matter **49**(4), 2362–2367 (1994).
21. C. Langhammer, M. Schwind, B. Kasemo, and I. Zorić, "Localized surface plasmon resonances in aluminum nanodisks," Nano Lett. **8**(5), 1461–1471 (2008).
22. A. Taguchi, Y. Saito, K. Watanabe, S. Yijian, and S. Kawata, "Tailoring plasmon resonances in the deep-ultraviolet by size-tunable fabrication of aluminum nanostructures," Appl. Phys. Lett. **101**(8), 081110 (2012).
23. S. Zhu, T. Y. Liow, G. Q. Lo, and D. L. Kwong, "Fully complementary metal-oxide-semiconductor compatible nanoplasmonic slot waveguides for silicon electronic photonic integrated circuits," Appl. Phys. Lett. **98**(2), 021107 (2011).
24. W. L. Barnes, "Surface plasmon–polariton length scales: a route to sub-wavelength optics," J. Opt. A, Pure Appl. Opt. **8**(4), S87–S93 (2006).
25. A. D. Rakic, A. B. Djurisic, J. M. Elazar, and M. L. Majewski, "Optical properties of metallic films for vertical-cavity optoelectronic devices," Appl. Opt. **37**(22), 5271–5283 (1998).
26. H. R. Philipp, "Optical properties of silicon nitride," J. Electrochem. Soc. **120**(2), 295–300 (1973).
27. A. V. Zayats and I. I. Smolyaninov, "Near-field photonics: surface plasmon polaritons and localized surface plasmons," J. Opt. A, Pure Appl. Opt. **5**(4), S16–S50 (2003).
28. L. Yin, V. K. Vlasko-Vlasov, A. Rydh, J. Pearson, U. Welp, S.-H. Chang, S. K. Gray, G. C. Schatz, D. B. Brown, and C. W. Kimball, "Surface plasmons at single nanoholes in Au films," Appl. Phys. Lett. **85**(3), 467–469 (2004).

1. Introduction

Confining light into a deep subwavelength scale has made surface plasmon polaritons (SPPs) attractive to the fields of modern optics, particularly in metamaterial studies [1–5], super-resolution imaging [6–8], optical trapping [9, 10], and transformation plasmonics [11, 12]. The propagation of SPPs can be controlled by monitoring polarization of the incident light [13–15]. As quasi particles, SPPs also play an important role in the area of sub-wavelength optics and 2D optics [16, 17]. However, the widely used noble metals, e.g., gold and silver, generally do not perform well in the short visible wavelength as compared to longer visible and infrared wavelength. This is mainly attributed to the interband transitions in the visible spectrum, which gives higher damping constant.

For this reason, aluminium is often proposed as an alternative material for plasmonics due to its lower damping constant in the UV and visible range, although with the disadvantage of oxidation [18]. The capability of aluminium for plasmonic applications has been theoretically studied [19, 20]. Experimentally, plasmon resonance in various aluminium nanostructures has been investigated [21, 22], and the feasibility of plasmonic guiding in Al/SiO_2 material system had been discussed [23]. However, there have been a few experimental studies about in-plane SPP properties on aluminium. In this paper, we report SPP propagation in the Al/air and Al/Si_3N_4/air structures for short visible wavelength. The Si_3N_4 layer in the Al/Si_3N_4/air structures is found capable of modifing SPP wavelength and loss in addition to preventin native oxidation of aluminum.

2. Structure design and principles

In the near field optics, the propagation of surface plasmon polaritons (SPPs) is characterized by surface plasmon wavelength (λ_{SPP}). For an incident light of wavelength $\lambda_{0,}$ the dispersion relation of SPPs along the metal-dielectric interface is given by [24]:

#243719 Received 30 Jun 2015; revised 2 Aug 2015; accepted 14 Aug 2015; published 21 Aug 2015

$$\lambda_{spp} \cong \lambda_0 \sqrt{\frac{\varepsilon_d + \varepsilon_m'}{\varepsilon_d \varepsilon_m'}} \tag{1}$$

where ε_m' and ε_d are the real permittivity of the metal and dielectric, respectively. In the case where the metal is highly plasmonic, $|\varepsilon_m'| >> \varepsilon_d$, Eq. (1) can be simplified as

$$\lambda_{SPP} \approx \lambda_0 (\varepsilon_d)^{-1/2} \tag{2}$$

which suggests that changing dielectric permittivity can readily tune the SPP wavelength.

However, the dielectric permittivity as perceived by the propagating SPP may not be the same as the bulk permittivity of the dielectric, particularly when the thickness of the dielectric film is smaller than the SPP penetration depth in the dielectric ($t < \delta_d$). This is expected as the SPP electric field overlaps with both dielectric and air, which gives an averaged permittivity according to its overlap integral. The SPP penetration depth in the metal (δ_m) and dielectric (δ_d) are expressed as [24]

$$\delta_m = \frac{1}{k_0} \left| \frac{\varepsilon'_m + \varepsilon_d}{\varepsilon'^2_m} \right|^{\frac{1}{2}}, \ \delta_d = \frac{1}{k_0} \left| \frac{\varepsilon'_m + \varepsilon_d}{\varepsilon_d^2} \right|^{\frac{1}{2}} \tag{3}$$

which, in highly plasmonic metal case (such as Al), can be further simplified into the following

$$\delta_m \cong \frac{1}{k_0} \frac{\sqrt{\varepsilon_d}}{|\varepsilon'_m|}, \ \delta_d \cong \frac{1}{k_0} \frac{\sqrt{|\varepsilon'_m|}}{\varepsilon_d} \tag{4}$$

where k_0 is the wave vector of the incident light in the vacuum.

It is clear that the SPP wavelength can be accurately predicted by Eq. (1) when the thickness of the dielectric film is thicker than the SPP penetration depth ($t > \delta_d$). However, when the dielectric thickness is smaller than the SPP penetration depth ($t < \delta_d$), the SPP wavelength would be longer than that calculated from Eq. (1). The loss and damping constant will also change as the film thickness is changed. As the leakage increases from the insulator-air interface, the direct measurement becomes possible. In our work, Silicon Nitride (Si_3N_4) was chosen for the dielectric layer. The SPP penetration depth in Si_3N_4 is deduced as $\delta_d \sim 90$ nm for the incidenct wavelength of $\lambda_0 = 473$ nm. Figure 1(a) shows the schematic of the Al/Si_3N_4/air structures with 80 nm thick aluminium and varied thickness of the Si_3N_4 layer.

Figures 1(b) and 1(c) show the simulated electric field distributions in z-y plane of the Al-Air structure (80 nm Al) and a typical MIA structure (80 nm Al and 40 nm Si_3N_4), respectively. The SPPs are excited by linearly polarized light of 473 nm at normal incidence through a slot opening which is about 100 nm wide. The input of the incident electric field is 1 Vm^{-1}, and the permittivities are $-30.498 + 7.727i$ for Al, 4.17 for Si_3N_4 and 1 for air at the incident wavelength of $\lambda_0 = 473$ nm [25, 26]. As shown from the figures, the SPPs excited by the incident light from the air slit propagate along the y and –y directions symmetrically and the field intensity decay along the propagation directions. It is also seen that for the structure with the 40 nm Si_3N_4 layer, the SPP field distribution and wavelength are different from those of the structure without the Si_3N_4 layer. To study the effects of the dielectric layer above the aluminium film, the E_z field distributions of the Al/Si_3N_4/air structures with same Al thickness (80 nm) but varied thickness of the Si_3N_4 layers from 20 nm to 60 nm are calculated and plotted in Fig. 1(d), where the vertical dash lines are used to indicate the wave fronts of these SPPs. It is clearly seen that the SPP wavelength shrinks with the increase of Si_3N_4 thickness, which is accompanied by the increasing propagation loss.

#243719 Received 30 Jun 2015; revised 2 Aug 2015; accepted 14 Aug 2015; published 21 Aug 2015

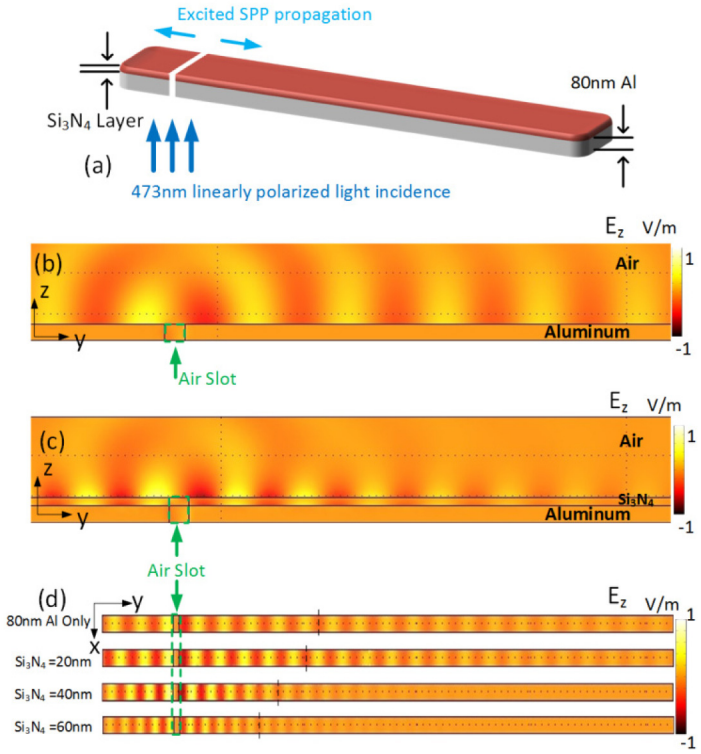

Fig. 1. (a) Schematic diagram of an aluminium based MIA structure. (b) Simulated E_z of the MIA structure consisting of 80nm Aluminium film and Air at z-y plane. (c) Simulated E_z of the MIA structure consisting of 80nm Aluminium film, 40nm Si_3N_4 film and Air at z-y plane. (d) E_z distributions in x-y plane at Si_3N_4/Air interface of the MIA structures with different thicknesses of Si_3N_4 layer above the 80nm Al film. The dashed straight lines are used to indicate the wavefronts of SPPs of the MIA structures.

For more details of SPP propagation in MIA structure, Fig. 2(a) shows the damping constant of E_z fields corresponding to 4 different Si_3N_4 thicknesses. As apparent from Fig. 2(a), for all the MIA structures studied, the decay becomes progressively faster as the Si_3N_4 thickness is increased. This observation is consistent with Eq. (4) which describes the relation between permittivity and the SPP penetration depth. Assuming that the Si_3N_4 is well below its skin depth ($t < 90$ nm) where the effective permittivity depends on the film thickness, one can see that increasing Si_3N_4 thickness gives higher effective Si_3N_4 permittivity, which according to Eq. (4) leads to the increase (decrease) of δ_m (δ_d). This in turn gives increased overlap between the field and metal, translating to higher propagation loss. On the other hand, decreasing Si_3N_4 thickness translates into increasing overlap between the field and the dielectric, resulting in lower propagation loss. To have quantitative description for the decay, the SPP propagation can be expressed as [27]:

$$E_z(y) = E_{z0} e^{ik_y' y} e^{-k_y'' y} = E_{z0} e^{ik_y' y} e^{\alpha_{SPP} y} \tag{5}$$

where α_{SPP} is the electric field decay rate of SPPs propagating in y direction which can be derived from the E_z field damping and shown in Fig. 2(b).

The SPP wavelength as a function of Si_3N_4 thickness is presented in Fig. 2(b), where the wavelength has shrunk from 430 nm to 265 nm as the Si_3N_4 thickness is increased from 20 nm to 60 nm. This also corresponds to the increase of the effective index of the dielectric materials which is consistent to Eq. (2), as shown in Fig. 2(b).

#243719 Received 30 Jun 2015; revised 2 Aug 2015; accepted 14 Aug 2015; published 21 Aug 2015

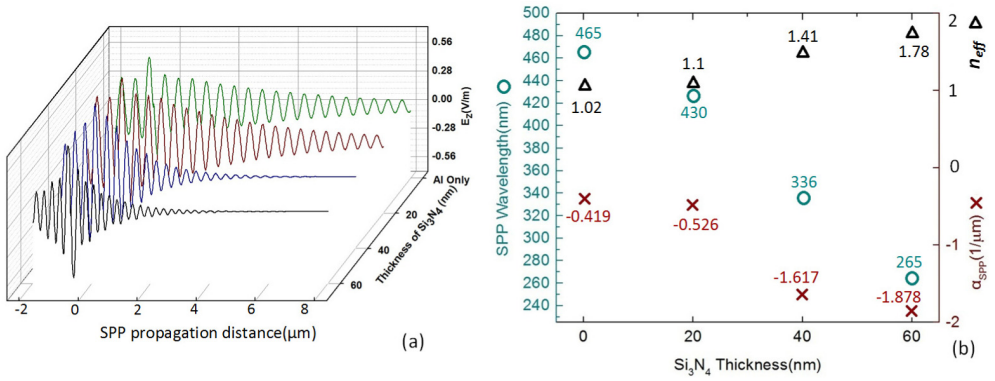

Fig. 2. (a) Damping of electric field E_z at Si_3N_4/Air interface of the MIA structures consisting of 80nm aluminium film and varied thickness of Si_3N_4 film. (b) SPP wavelength (circle), effective refraction index n_{eff} (triangle) and decay rate (cross) as a function of thickness t of Si_3N_4 film. Here, n_{eff} approximately follows a polynomial relation, $n_{eff} = 1.01 + 0.0021t + 1.81 \times 10^{-4}t^2$.

3. Experimental verification

For experimental verification, the thickness of Si_3N_4 film cannot be too large as it will weaken the near-field signals on the top Si_3N_4 surface, making the NSOM characterization difficult. For the above reason, we fabricated two structures, one of which has only 80 nm Al and the other has 80nm Al/ 20nm Si_3N_4 on quartz substrate, as illustrated in Figs. 3(a) and 3(b). The top views of the two structures with fabricated gratings are shown in Figs. 3(c) and 3(d).

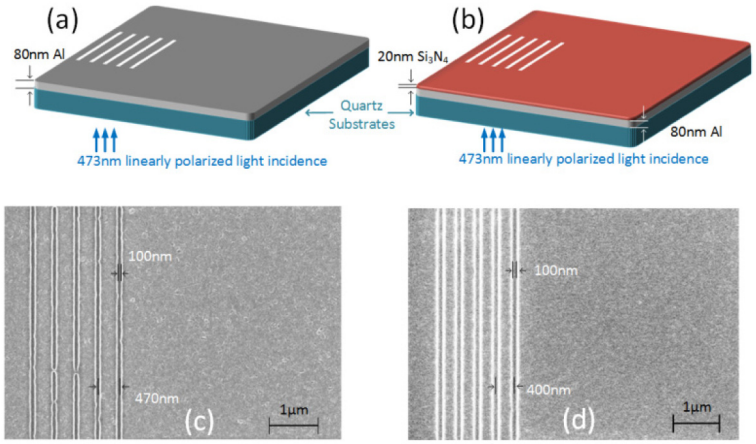

Fig. 3. Schematic of (a) 80-nm thick aluminium film on quartz substrate (Sample 1), and (b) 20-nm thick Si_3N_4/80-nm thick Al on quartz substrate (Sample 2). The SEM images of these samples integrated with grating coupler: (c) Sample 1, and (d) Sample 2.

The Al sputtering was carried out with 30W DC power and 6.4 sccm Argon gas, while the Si_3N_4 sputtering was carried out with 80W RF power and 5.5 sccm Argon gas. There was no break of vacuum between the deposition of the two layers. The thicknesses of both layers were verified by a surface profiler. The gratings were then fabricated by focused ion beam (Carl Zeiss AURIGA crossbeam FIB-SEM workstation) using 30 keV at 120pA beam current. The slit width of the gratings is 100 nm, while the periodicities are 470 nm (sample 1) and 400 nm (sample 2). The coupling efficiency varies with the number of grating slit and periodicity. We made 5 grating slits by considering the laser spot size. The periodicity for

#243719 Received 30 Jun 2015; revised 2 Aug 2015; accepted 14 Aug 2015; published 21 Aug 2015

sample 2 is mismatched with the simulated SPP wavelength. Such mismatch does not significantly affect our analysis as it has no effect on SPP wavelength although the field intensity is not as strong as in the matched case.

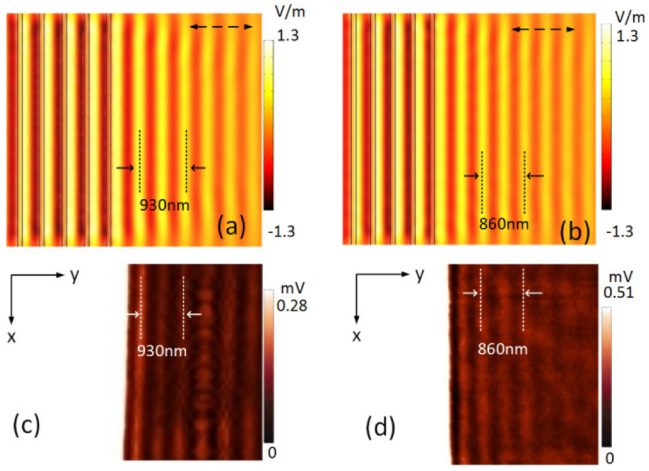

Fig. 4. E_z distributions in x-y plane of (a) sample 1 and (b) sample 2 for y polarized incidence. NSOM images of (c) sample 1 and (d) sample 2. The dashed arrows in (a) and (b) denote the direction of linear polarization.

The electric field distributions were measured using a near-field scanning optical microscope (NSOM). The linearly polarized 473nm laser was normally incident from the bottom of the quartz substrate. We used a photomultiplier tube (PMT) for signal detection and amplification. The NSOM probe tip (aluminium-coated) is less than 100 nm in diameter and it is positioned about 10 nm above the sample surface, based on shear-force feedback mechanism.

The SPP near field patterns are shown in Fig. 4, which results from the interference between the in-plane SPP fields and the transmitted out-of-plane incident beam [14, 28]. The SPP wavelengths can be deduced as the distance between the fringes, $\lambda_{spp} = d/(q - 1)$, where d is the distance between q fringes. The SPP wavelengths in Figs. 4(c) and 4(d) are about 465 ± 5 nm for the sample with 80nm Aluminium only and about 430 ± 5 nm for the sample with 80nm Aluminium film and 20nm Si_3N_4 coating. The FEM simulation and NSOM results are also presented in Figs. 4(a) and 4(b), where the fringing can be seen for each condition, showing excellent agreement between the measured values and simulation. Finally, we compare our experimental findings with our simulations in Fig. 2(b), showing excellent agreement.

4. Conclusion

We proposed aluminium based MIA structures and studied SPP propagation characteristics theoretically and experimentally. Such structures can be used to excite and propagate SPPs of wavelengths from 465 nm to about 265 nm by varying the thickness of a coated Si_3N_4 layer up to 60 nm, which provides an alternative way to manipulate in-plane SPPs. In addition, with a coated thin Si_3N_4 layer, the oxidation of Al can be prevented to a certain extent. We believe that the presented aluminium based MIA structures have potential applications in nanophotonics, such as super-resolution focusing and 2D optics.

Acknowledgments

This work is supported by the Ministry of Education (RG86/13), A*Star (1220703063), the Economic Development Board (NRF2013SAS-SRP001-019), Singapore and Asian Office of Aerospace Research and Development (FA2386-14-1-0013). The authors thank X. Shen, B.

Cao and C. Zou from SPMS, Nanyang Technological University for their assistance in FIB fabrication.

#243719 Received 30 Jun 2015; revised 2 Aug 2015; accepted 14 Aug 2015; published 21 Aug 2015